A Family Picture: Tracing the Dynamical Path of the Structural Properties of Multiple Populations in Globular Clusters

Emanuele Dalessandro[1] , M. Cadelano[1,2] , E. Vesperini[3], S. Martocchia[4,5], F. R. Ferraro[1,2] , B. Lanzoni[1,2] , N. Bastian[5] , J. Hong[3,6], and N. Sanna[7]

[1] INAF—Astrophysics and Space Science Observatory Bologna, Via Gobetti 93/3 I-40129 Bologna, Italy; emanuele.dalessandro@inaf.it
[2] Dipartimento di Fisica e Astronomia, Via Gobetti 93/2 I-40129 Bologna, Italy
[3] Department of Astronomy, Indiana University, Swain West, 727 E. 3rd Street, Bloomington, IN 47405, USA
[4] European Southern Observatory, Karl-Schwarzschild-Straβe 2, D-85748 Garchin bei Munchen, Germany
[5] Astrophysics Research Institute, Liverpool John Moores University, 146 Brownlow Hill, Liverpool L3 5RF, UK
[6] Kavli Institute for Astronomy and Astrophysics, Peking University, Yi He Yuan Lu 5, HaiDian District, Beijing 100871, People's Republic of China
[7] INAF—Osservatorio Astrofisico di Arcetri, Largo Enrico Fermi 5, I-50125 Firenze, Italy
Received 2019 July 26; revised 2019 September 13; accepted 2019 September 19; published 2019 October 11

Abstract

We studied the spatial distributions of multiple stellar populations (MPs) in a sample of 20 globular clusters (GCs) spanning a broad range of dynamical ages. The differences between first-population (FP) and second-population (SP) stars were measured by means of the parameter A^+, defined as the area enclosed between their cumulative radial distributions. We provide the first purely observational evidence of the dynamical path followed by MPs from initial conditions toward a complete FP–SP spatial mixing. Less dynamically evolved clusters have SP stars more centrally concentrated than FPs, while in more dynamically evolved systems the spatial differences between FP and SP stars decrease and eventually disappear. By means of an appropriate comparison with a set of numerical simulations, we show that these observational results are consistent with the evolutionary sequence expected by the long-term dynamical evolution of clusters forming with an initially more centrally concentrated SP subsystem. This result is further supported by the evidence of a trend between A^+ and the stage of GC dynamical evolution inferred by the ratio between the present-day and the initial mass of the cluster.

Unified Astronomy Thesaurus concepts: Globular star clusters (656); Star clusters (1567); Hertzsprung Russell diagram (725); Giant branch (650); HST photometry (756); Broad band photometry (184); Dynamical evolution (421)

1. Introduction

The presence of subpopulations differing in terms of their light-element abundances (e.g., He, C, N, O, Na, Mg, Al) while having the same iron (and iron-peak) content (hereafter multiple stellar populations—MPs) is a key general property of globular clusters (GCs; see Bastian & Lardo 2018 for a recent review). In fact, MPs are observed in nearly all old ($t > 2$ Gyr) and relatively massive systems ($M > 10^4 M_\odot$), both in the Milky Way and in external galaxies (e.g., Mucciarelli et al. 2008; Larsen et al. 2014; Dalessandro et al. 2016).

MPs are characterized by specific light-element chemical abundance patterns like C–N, Na–O, Mg–Al anticorrelations. Stars sharing the same chemical abundances as the surrounding field stars (Na-poor/O-rich, CN-weak) are commonly classified as first population (FP), while Na-rich/O-poor, CN-strong stars are referred to as second population (SP). Light-element chemical abundance variations can have an impact on both the stellar structure and atmosphere thus producing a variety of features (such as broadening or splitting of different evolutionary sequences) in color–magnitude diagrams (CMDs) when appropriate optical and near-UV bands are used (Sbordone et al. 2011; Piotto et al. 2015; Milone et al. 2017). It has been shown that the fraction of SP stars and the amplitude of the light-element anticorrelations depends on the present-day cluster mass (e.g., Carretta et al. 2010; Schiavon et al. 2013; Milone et al. 2017), with relatively small systems ($M < 10^5 M_\odot$) typically having a fraction of ~40%–50% of SP stars, which then increases to ~90% for the most massive ones. Light-element inhomogeneities appear to decrease also as a function of cluster age, becoming undetectable for a cluster younger than ~2 Gyr (Martocchia et al. 2018a), although the exact role of age is currently not clear yet.

MPs are believed to form during the very early epochs of GC formation and evolution (~10–100 Myr; but see Martocchia et al. 2018b for recent observational constraints on this aspect). A number of scenarios have been proposed over the years to explain their formation; however, their origin is still strongly debated (Decressin et al. 2007; D'Ercole et al. 2008; Bastian et al. 2013; Denissenkov & Hartwick 2014; Gieles et al. 2018; Calura et al. 2019).

The kinematical and structural properties of MPs can provide key insights into the early epochs of GC evolution and formation. In fact, one of the predictions of MP formation models (see, e.g., D'Ercole et al. 2008) is that SP stars form a centrally segregated stellar subsystem possibly characterized by a more rapid internal rotation (Bekki 2011) than the more spatially extended FP system. Although the original structural and kinematical differences between FP and SP stars are gradually erased during GC long-term dynamical evolution (see, e.g., Vesperini et al. 2013; Hénault-Brunet et al. 2015; Miholics et al. 2015; Tiongco et al. 2019), some clusters are expected to still retain some memory of these initial differences in their present-day properties.

Indeed, sparse and inhomogeneous observations show that MPs are characterized by quite remarkable differences in their relative structural parameters/radial distributions (Lardo et al. 2011; Dalessandro et al. 2016; Massari et al. 2016; Simioni et al. 2016), different degrees of orbital anisotropy (Richer et al. 2013;

Table 1
GC A^+ Info

Cluster	A_2^+	ϵ	$\log(t)$	$\log(t_{rh})$	M_{PD} ($\times 10^5 M_\odot$)	r_h ($''$)	R_{GC} (kpc)	[Fe/H]
NGC 121	−0.047	0.001	10.021	9.53	3.42	27.0	61.9	−1.28
NGC 288	−0.045	0.002	10.097	9.32	1.16	133.8	12.0	−1.32
NGC 362	−0.040	0.001	10.061	8.93	3.45	49.2	9.4	−1.26
NGC 1261	0.023	0.001	10.061	9.12	1.67	40.8	18.1	−1.27
NGC 1851	−0.032	0.001	10.079	8.82	3.02	30.6	16.6	−1.18
NGC 1978	−0.081	0.003	9.301	9.02	2.00	31.1	49.6	−0.35
NGC 2808	−0.029	0.001	10.079	9.15	7.42	48.0	11.1	−1.14
NGC 5272	−0.059	0.001	10.097	9.79	3.94	138.6	12.0	−1.5
NGC 5286	−0.013	0.001	10.114	9.11	4.01	43.8	8.9	−1.69
NGC 6093	0.056	0.001	10.130	8.80	2.49	36.6	3.8	−1.75
NGC 6101	−0.003	0.001	10.114	9.22	1.27	63.0	11.2	−1.98
NGC 6362	−0.010	0.002	10.097	9.20	1.47	123.0	5.1	−0.99
NGC 6584	0.033	0.002	10.088	9.02	0.91	43.8	7.0	−1.50
NGC 6624	0.016	0.002	10.114	8.71	0.73	49.2	1.2	−0.44
NGC 6637	−0.028	0.001	10.097	8.82	2.45	50.4	1.7	−0.64
NGC 6652	0.029	0.003	10.122	8.39	0.57	28.8	2.7	−0.81
NGC 6681	−0.031	0.003	10.114	8.65	1.13	42.6	2.2	−1.62
NGC 6715	−0.107	0.001	10.079	9.93	14.1	49.2	18.9	−1.49
NGC 6717	0.080	0.004	10.114	8.22	0.36	48.0	2.4	−1.26
NGC 6934	0.000	0.002	10.079	9.04	1.17	41.4	12.8	−1.47

Note. Ages are from Dotter et al. (2010) for all clusters but NGC1978 and NGC121 (Martocchia et al. 2018a and Dalessandro et al. 2016, respectively). Masses for Galactic GCs are from Baumgardt & Hilker (2018); for NGC 121 we used values from Glatt et al. (2011) and for NGC 1978 from Krause et al. (2016). Relaxation times come from Harris (1996) and Glatt et al. (2011) for NGC 121 and the present work for NGC 1978.

Bellini et al. 2015), different rotation amplitudes (Cordero et al. 2017), and significantly different binary fractions (Lucatello et al. 2015; Dalessandro et al. 2018b). However, so far the lack of a homogeneous and self-consistent study of MP kinematical and structural properties for a statistically representative sample of clusters has hampered our ability to build an observational picture to test and constrain models for the formation and evolutionary history of GCs.

In this Letter we use the A^+ parameter (originally introduced for blue straggler star studies; Alessandrini et al. 2016; Lanzoni et al. 2016) to quantify the differences in the radial distributions of FP and SP stars for a large sample of GCs in different stages of their dynamical evolution measured here by the ratio $N_h = t/t_{rh}$ between the cluster age t and its current half-mass relaxation times (t_{rh}). A comparison of our results with those of numerical simulations following the dynamical evolution and spatial mixing of MPs allows us to draw, for the first time, an observational picture of the evolutionary path of FP and SP structural properties.

2. Sample Definition and Population Selection

For the present analysis we mainly used the publicly available photometric catalogs of Galactic GCs presented in Nardiello et al. (2018; see also Piotto et al. 2015) and observed through proposals GO-13297, GO-12605, and GO-12311 (PI: Piotto) with the *Hubble Space Telescope* (*HST*) WFC3/UVIS camera in the F275W, F336W, and F438W bands and with the *HST* ACS/ WFC under proposal GO-10775 (PI: Sarajedini) in the F606W and F814W filters. We limited our analysis only to systems for which the available *HST* catalogs cover at least 2 cluster half-light radii (r_h) allowing us to probe a region large enough to capture possible differences between the SP and FP spatial distributions.

With the adopted selection we are able to include in our sample 15 GCs, most of which have $N_h > 7$–8. To further extend our analysis and include clusters with smaller values

of N_h, which is essential for the goals of our study, we complemented our data set with the wide-field photometric catalog (that includes U, B, V, and I bands) published by Stetson et al. (2019) for the low-mass cluster NGC 288, the Strömgren photometry of NGC 5272 (M3) presented by Massari et al. (2016), and the combined *HST* and ground-based wide-field catalog of NGC 6362 published in Dalessandro et al. (2014). Finally, we also included two extragalactic systems, namely, NGC 121 in the Small Magellanic Cloud and NGC 1978 in the Large Magellanic Cloud. The *HST* photometry of these two clusters was presented in Dalessandro et al. (2016) and Martocchia et al. (2018a), respectively. It is important to stress that to make the MP separation and selection as straightforward/clear as possible, only clusters with inter-mediate-high metallicity,[8] low reddening, relatively low field contamination, and with a well-populated red giant branch (RGB) were added to the initial list of 15 GCs. With such a combination our sample counts 20 GCs covering (see Table 1) a wide range in metallicity (−0.4 < [Fe/H] < −2) and present-day mass ($3.6 \times 10^4 M_\odot < M < 1.4 \times 10^6 M_\odot$), which are well representative of the population of Galactic and Magellanic Cloud GCs, with the exception of the lower-mass systems in the Clouds. More importantly to the present analysis, the sample covers the full range of dynamical stages derived for Galactic and Magellanic Cloud clusters ($1 < N_h < 80$).

For the clusters for which we used the photometric catalogs published by Nardiello et al. (2018), MPs were selected along the RGB in the ($\Delta_{F275W,F814W}$, $\Delta_{F275W,F336W,F438W}$) diagram, the so-called "chromosome map," following the same approach used by Milone et al. (2017) and schematically shown in Figures 1(a1)–(a3). Briefly, we verticalized the distribution of RGB stars in the

---

[8] It is well known that the amplitude of color variations caused by the effect of light-element anticorrelations decreases with metallicity. Thus, photometric broadenings or splittings of the evolutionary sequences in the CMD are harder to detect in metal-poor systems.
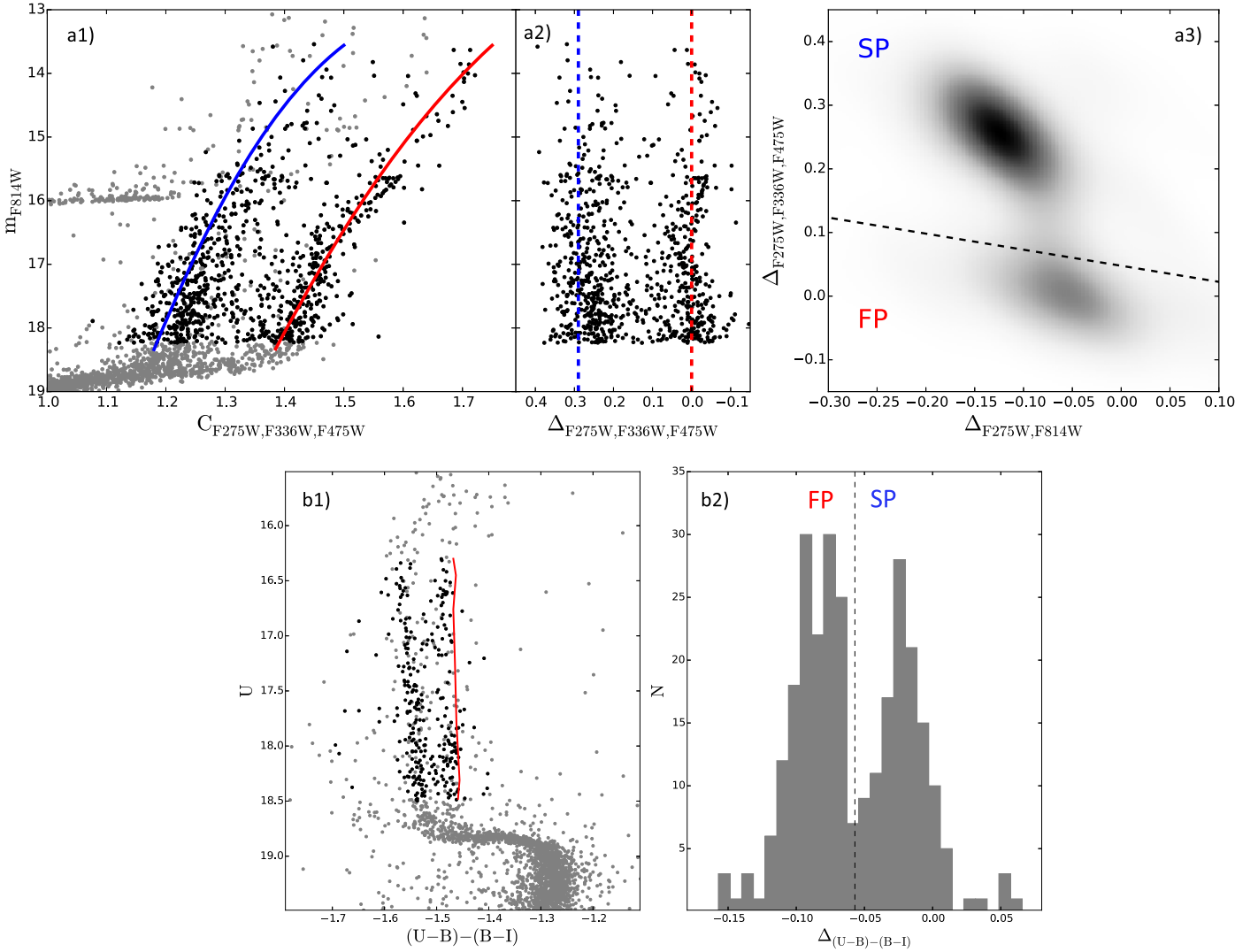
Figure 1. (a1) (m_{F814W}, $C_{F275W,F336W,F438W}$) CMD of NGC 6541. Data are from Nardiello et al. (2018). The red and blue lines represent the two fiducial lines at the edge of the RGB. Black dots are stars selected as described in Section 2. (a2) Verticalized m_{F814W}, $\Delta_{F275W,F336W,F428W}$ distribution of RGB stars with respect to the fiducial lines. (a3) The derived ($\Delta_{F275W,F814W}$, $\Delta_{F275W,F336W,F438W}$) diagram. The black dashed line marks the boundary between FP and SP stars. (b1) (U, $(U-B)-(B-I)$) CMD of NGC 288. Data are from Stetson et al. (2019). The red line represents the fiducial line at the bluer edge of the RGB. (b2) Distribution of the verticalized color $\Delta_{(U-B)-(B-I)}$. As before, the black dashed line marks the limit adopted to separate FP from SP stars.

(m_{F814W}, $C_{F275W,F336W,F438W}$) and (m_{F814W}, $m_{F275W} - m_{F814W}$) diagrams (where $C_{F275W,F336W,F438W} = (m_{F275W} - m_{F336W}) - (m_{F336W} m_{F438W})$) with respect to two fiducial lines at the blue and red edges of the RGB in both CMDs (Figure 1, panels (a1) and (a2)). The combination of the two verticalized distributions ($\Delta_{F275W,F814W}$ and $\Delta_{F275W,F336W,F438W}$) gives the "chromosome map" (Figure 1(a3)). Only stars with a membership probability >75% and with quality flags >0.9 in all bands were used (see Nardiello et al. 2018 for details).

For NGC 121, NGC 6362, M3, and NGC 1978 we adopted the same subpopulation selections described in Dalessandro et al. (2014, 2016), Massari et al. (2016), Martocchia et al. (2018a), respectively.

For the case of NGC 288, we used a two-step approach. For stars at a cluster-centric distance $R < 100''$ we used the *HST* catalog published by Nardiello et al. (2018) and the selection criteria described before. For the external region we first matched the ground-based catalog with *Gaia* DR2 data. Cluster bona fide stars were selected based on their *Gaia* proper motions. We assumed ($\mu_\alpha = 4.24$, $\mu_\delta = 5.65$) mas yr^{-1} as cluster mean motion (Gaia Collaboration et al. 2018), and we selected stars at distance $d < 1.5$ mas yr^{-1} in the vector-point diagram. RGB likely cluster members were verticalized in the (U, $(U-B)-(B-I)$) CMD with respect to a fiducial line on the blue edge of the RGB (Figure 1(b1); see also Monelli et al. 2013). The resulting distribution is clearly bimodal (panel (b2)). Stars redder/bluer than $\Delta_{(U-B)-(B-I)} = -0.55$ were selected as FP/SP stars.

It is important to note that, while in general, the adoption of different filter combinations for FP and SP classifications can introduce some bias, this is not the case for the specific targets in our sample for which both ground-based photometry and the *HST* "chromosome map" are available, namely, NGC 288, NGC 6362, and M3. In fact, we have verified, by using the stars in common between the available *HST* and wide-field catalogs, that there is a nice match between the two subpopulation selections, thus ensuring homogeneity of the different samples.
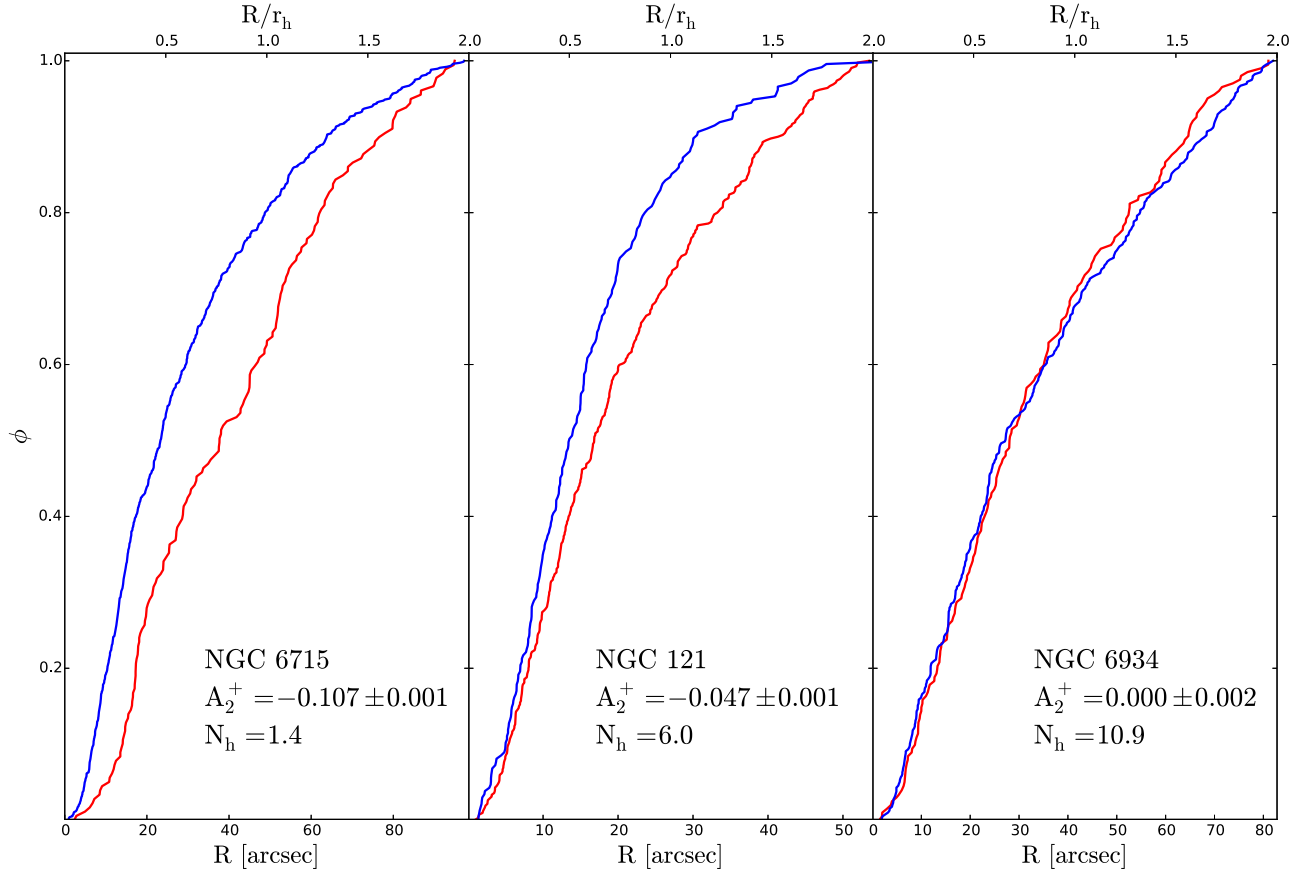
Figure 2. Cumulative radial distributions of FP (red) and SP (blue) for three representative clusters: M54 is one of the clusters with the smallest value of N_h in the sample, and it shows a very negative value of A_2^+, while NGC 6934 is an example of fully radial mixed cluster and NGC 121 is an intermediate case.

3. Radial Distribution of Multiple Populations and Empirical Derivation of the Parameter A^+

We derived the cumulative radial distributions of the selected subpopulations by using the cluster centers reported in Ferraro et al. (2012) and Lanzoni et al. (2016) and references therein for the clusters in common, and those listed in Goldsbury et al. (2010) for the other Galactic GCs. For NGC 121 and NGC 1978 we used the centers derived by Dalessandro et al. (2016) and Martocchia et al. (2018a), respectively.

In order to obtain a homogeneous measure of the differences between the SP and FP spatial distributions we have used the A^+ parameter introduced by Alessandrini et al. (2016) and Lanzoni et al. (2016) in the context of studying the spatial segregation of blue straggler stars. In our study A^+ is calculated as the area enclosed between the cumulative radial distributions of FP and SP stars, $\phi_{FP}(R)$ and $\phi_{SP}(R)$, respectively:

$$A^+(R) = \int_{R_{\min}}^{R} (\phi_{FP}(R') - \phi_{SP}(R'))dR', \qquad (1)$$

where R is the distance from the cluster center. With such a definition, a more centrally concentrated SP yields negative values of A^+. By construction A^+ depends on the considered cluster-centric distance and therefore a meaningful cluster-to-cluster comparison requires that the parameter is measured over equivalent radial portions in every system. As shown in numerical studies (see, e.g., Vesperini et al. 2013), spatial

mixing is achieved first in a cluster's inner regions and later in the cluster's outskirts. Therefore, capturing a complete dynamical picture of the mixing process in a given cluster would require a wide radial coverage possibly extending to the cluster's outermost regions, which retain memory of the initial spatial differences for a longer time. With this in mind, we decided to measure A^+ within 2 r_h from the cluster center (A_2^+). This limit represents a compromise between radial coverage and cluster sample size. We adopted the values of r_h reported by Harris (1996, 2010 version) for all the Galactic clusters, while we used Glatt et al. (2011) for NGC 121. For NGC 1978 we derived $r_h = 31\rlap{.}''5$ by fitting its number count density profile (derived by using the *HST* catalog) with a single-mass King (1966) model.

Uncertainties on the derived values of A^+ have been obtained by applying a jackknife bootstrapping technique (Lupton 1993). The results are reported in Table 1.

4. Results

The MP radial distributions in the targeted clusters appear to be quite different from one case to the other. However, in general we can identify two main behaviors: in about half of the sample, SP stars are more centrally concentrated than FPs, in the other clusters there is no significant difference between the FP and SP distributions. As a result, the derived values of A_2^+ cover a quite large range, from a minimum of $\sim -0.107 \pm 0.006$ for NGC 6715 (M54) to $\sim 0.080 \pm 0.016$ for NGC 6717 (Table 1). The cumulative radial distributions
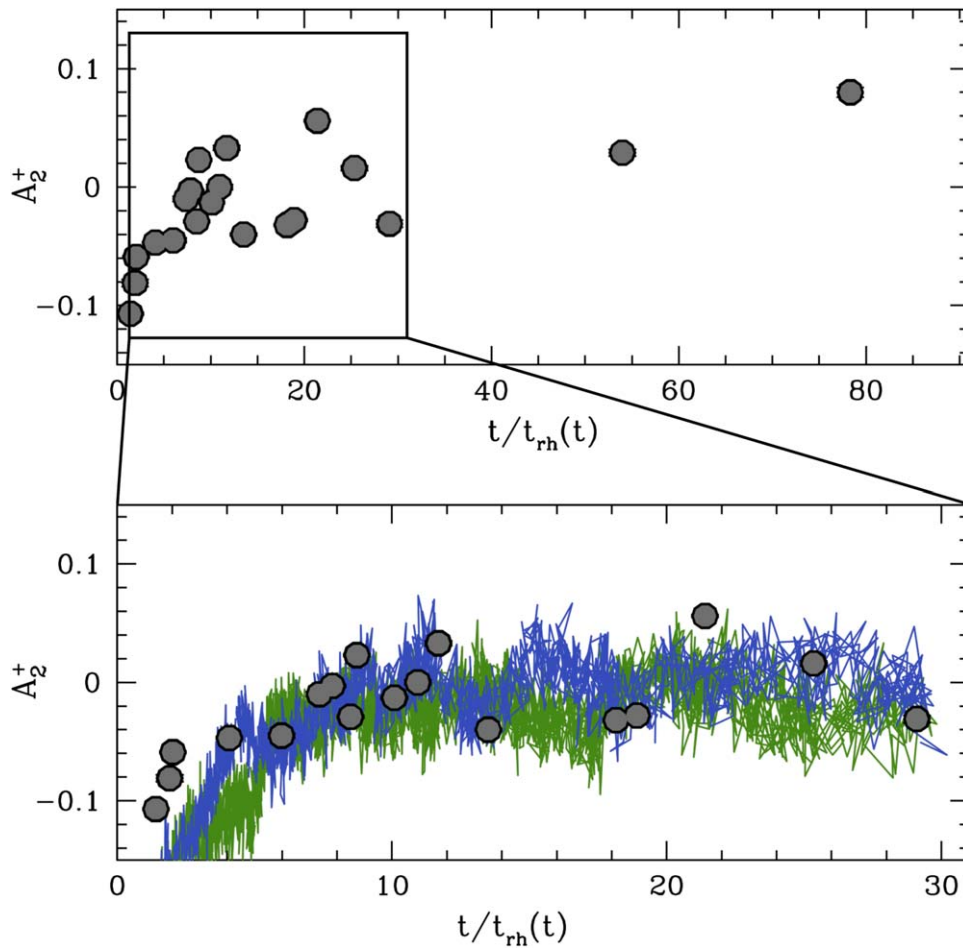
Figure 3. Upper panel: distribution of A_2^+ as a function of t/t_{rh} (N_h) for all the clusters in the sample. Bottom panel: zoom on the distribution of cluster with $N_h < 30$. Results from N-body models are overplotted to the observations. Blue and green curves represent models starting with an SP 5 and 10 times more centrally concentrated than FP, respectively.

for three systems with different behaviors are shown in Figure 2 as an example.

For every cluster we determined N_h by adopting the ages derived by Dotter et al. (2010) for Galactic GCs and by Martocchia et al. (2018a) and Glatt et al. (2011) for NGC 1978 and NGC 121, respectively, while the values of t_{rh} are taken from Harris (1996) and Glatt et al. (2011) for NGC 121. For NGC 1978 we derived $\mathrm{Log}(t_{rh}) = 9.02$ (where t_{rh} has been calculated as in Harris 1996). Figure 3 shows the distribution of A_2^+ as a function of N_h. The A_2^+ parameter increases almost linearly up to $N_h \sim 10$, reaching values close to 0 where FP and SP stars are (almost) fully radially mixed, then it shows an almost constant distribution for older dynamical ages up to $N_h \sim 80$.

The general trend shown in Figure 3 suggests that SP stars are significantly more concentrated than FPs in systems with $N_h < 8-10$, while MP radial distributions do not show significant differences for clusters in more advanced stages of their dynamical evolution (with $N_h > 10$). The only two exceptions are NGC 6093 (M80) and NGC 6717, which are the systems in the sample characterized by most positive values of A^+. The MP radial distribution of M80 has been analyzed in detail and extensively discussed in Dalessandro et al. (2018a).

To illustrate the expected evolution of A_2^+ as a function of N_h, in Figure 3 (bottom panel) we show the time evolution of A_2^+ obtained from N-body simulations following the long-term

dynamical evolution of two MP clusters in which the SP is initially 5 and 10 times more centrally concentrated than the FP one. The simulations start with 50,000 stars equally split between FP and SP and follow a cluster internal evolution and mass loss due to the combined effects of two-body relaxation and tidal truncation. The simulations have been presented in Vesperini et al. (2018) and Dalessandro et al. (2018a) and we refer to those papers for further details. Here we use these simulations to explore the role of internal two-body relaxation and the interaction of the external tidal field of the host galaxy in the evolution of A_2^+ as a function of N_h. We point out that the simulations presented here are still idealized and not meant to model any specific cluster in detail, but they serve to illustrate the general evolutionary trend expected for A_2^+ as the SP and the FP mix. Detailed models aimed at reproducing the properties of specific clusters would require more realistic simulations.

Since the N-body models start with a more centrally concentrated SP radial distribution, the simulations have initially negative values of A_2^+. As the FP and SP stellar subsystems evolve (i.e., N_h increases) the two populations gradually mix and, as a consequence, A_2^+ increases evolving toward zero, which represents the value corresponding to a fully radially mixed configuration. Although the simulations are still simplified, they follow the general A_2^+ trends. This suggests that the different shapes of MP radial distributions and
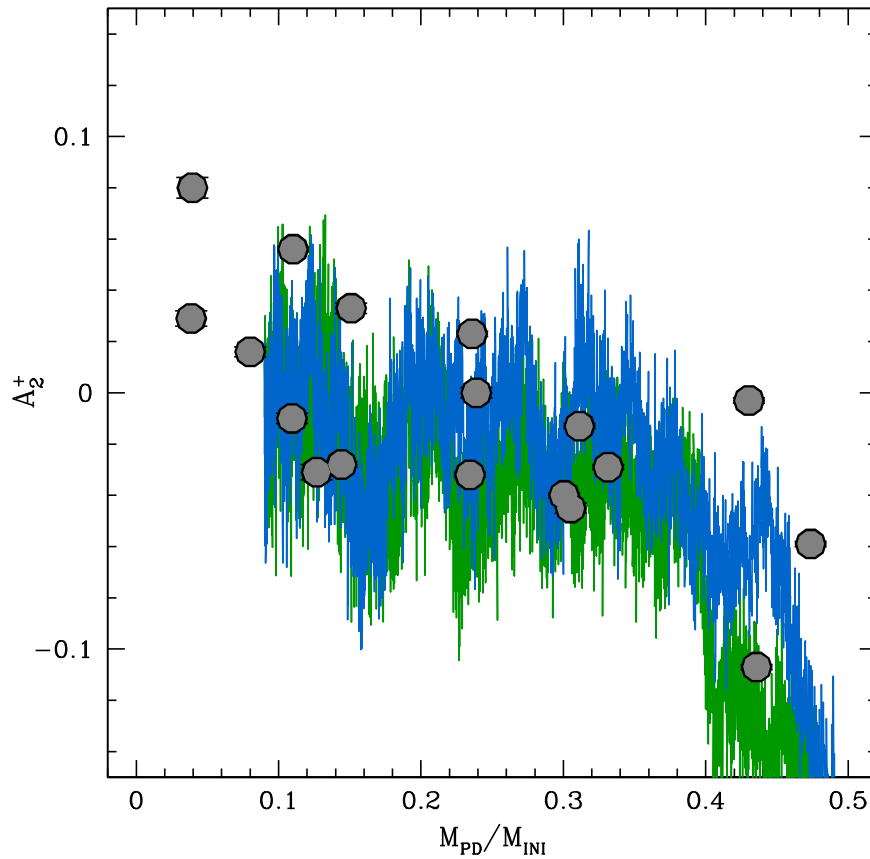
Figure 4. Distribution of A_2^+ as a function of the ratio between the present-day and the initial cluster mass (M_{PD}/M_{ini}) obtained by Baumgardt et al. (2019). Blue and green curves represent the same models shown in Figure 3.

the trend found in this study are the result of the effects of the long-term dynamical evolution in clusters formed with an initially more centrally concentrated SP stellar subsystem.

It is important to note that in this comparison FP and SP are assumed to have the same He abundance or only small mean variations ($\Delta Y < 0.01$–0.02). Indeed, this is observed to be the case in the vast majority of GCs (see, for example, Dalessandro et al. 2013) with only a few exceptions in our sample, such as NGC 2808 (Piotto et al. 2007), M80 (Dalessandro et al. 2018a), NGC 7078 (M15), and M54 (Milone et al. 2018).

In Figure 4 we show the dependence of A_2^+ on the ratio between the present-day and the initial cluster mass (M_{PD}/M_{ini}), as estimated by Baumgardt et al. (2019). Although it is important to emphasize that much caution should be used in taking M_{PD}/M_{ini} ratios at face value because of the underlying strong assumptions made to derive them, and the possible missing contribution of related effects,[9] they nevertheless provide a measure of the evolutionary stage of a cluster and its degree of mass loss due to two-body relaxation and the interaction with the Galactic potential. Our data show a significant correlation (Spearman's rank correlation coefficient $r \sim -3.7$) between A_2^+ and M_{PD}/M_{ini}: clusters with a small value of M_{PD}/M_{ini} (i.e., systems that lost a larger fraction of their original mass) tend to have their MPs spatially mixed. Interestingly, such a behavior is also reproduced (at least qualitatively) by our N-body models, thus demonstrating that

the fraction of mass lost is a key ingredient of the MP spatial mixing process (see the discussion on this issue in Vesperini et al. 2013; Hénault-Brunet et al. 2015; Miholics et al. 2015).

Not surprisingly (because of the known dependence with the dynamical parameters used before) we find that A_2^+ nicely anticorrelates with the present-day mass (M_{PD} from Baumgardt & Hilker 2018).

5. Conclusions

The variations of the MP radial distributions as a function of the evolutionary stage in the clusters' dynamical evolution shown in this Letter provides the first observational evidence of the dynamical path followed by MPs from their initial conditions toward a complete spatial mixing.

Our study has revealed a clear trend of the difference between the SP and FP spatial radial distributions (A_2^+) and GC dynamical evolution, as constrained by both the ratio of a cluster's age to its half-mass relaxation timescale and the ratio of a cluster's present-day to its initial mass. This is the first time that observational constraints on the evolutionary path of the MP structural differences are set and put in the framework of star cluster dynamical evolution.

Although additional work is needed to constrain in detail the initial physical properties of MPs both observationally and in the context of different theoretical formation models, our results provide a global view of the evolution of the MP structural properties. They lend support to an interpretation of the different degrees of spatial mixing observed in various clusters in terms of dynamical evolution of systems in which

---

[9] Examples of the missing contribution are early time-variation of the external potential or other mechanisms related to a cluster's response to early evolutionary processes (e.g., gas expulsion, mass loss due to stellar evolution, interactions with giant molecular clouds).

the SP formed more centrally concentrated than the FP. At the same time, the empirical evolutionary sequence found in our analysis also provides a key constraint for models exploring the long-term dynamics of MPs, which is an important aspect of the study of MP clusters.

The result presented here has important implications also for the interpretation of other kinematical features observed in MPs, such as their rotation patterns and anisotropy profiles, and therefore is key to shedding light on the physical initial conditions brought to the formation of MPs.

An extension of the present analysis, mainly including a larger sample of less dynamically evolved clusters, is needed to further confirm and sharpen the picture emerging from our study.

In addition, a systematic combination of structural and kinematic information of MPs is an essential step to properly interpreting observational data, as well as testing the key elements of theoretical scenarios of cluster formation and evolution.

ORCID iDs

Emanuele Dalessandro https://orcid.org/0000-0003-4237-4601
M. Cadelano https://orcid.org/0000-0002-5038-3914
F. R. Ferraro https://orcid.org/0000-0002-2165-8528
B. Lanzoni https://orcid.org/0000-0001-5613-4938
N. Bastian https://orcid.org/0000-0001-5679-4215

References

Alessandrini, E., Lanzoni, B., Ferraro, F. R., Miocchi, P., & Vesperini, E. 2016, ApJ, 833, 252
Bastian, N., Lamers, H. J. G. L. M., de Mink, S. E., et al. 2013, MNRAS, 436, 2398
Bastian, N., & Lardo, C. 2018, ARA&A, 56, 83
Baumgardt, H., & Hilker, M. 2018, MNRAS, 478, 1520
Baumgardt, H., Hilker, M., Sollima, A., et al. 2019, MNRAS, 482, 5138
Bekki, K. 2011, MNRAS, 412, 2241
Bellini, A., Renzini, A., Anderson, J., et al. 2015, ApJ, 805, 178
Calura, F., D'Ercole, A., Vesperini, E., Vanzella, E., & Sollima, A. 2019, MNRAS, 489, 3269
Carretta, E., Bragaglia, A., Gratton, R. G., et al. 2010, A&A, 516, A55
Cordero, M. J., Hénault-Brunet, V., Pilachowski, C. A., et al. 2017, MNRAS, 465, 3515
Dalessandro, E., Cadelano, M., Vesperini, E., et al. 2018a, ApJ, 859, 15
Dalessandro, E., Ferraro, F. R., Massari, D., et al. 2013, ApJ, 778, 135
Dalessandro, E., Lapenna, E., Mucciarelli, A., et al. 2016, ApJ, 829, 77
Dalessandro, E., Massari, D., Bellazzini, M., et al. 2014, ApJL, 791, L4
Dalessandro, E., Mucciarelli, A., Bellazzini, M., et al. 2018b, ApJ, 864, 33
Decressin, T., Charbonnel, C., & Meynet, G. 2007, A&A, 475, 859
D'Ercole, A., Vesperini, E., D'Antona, F., McMillan, S. L. W., & Recchi, S. 2008, MNRAS, 391, 825
Denissenkov, P. A., & Hartwick, F. D. A. 2014, MNRAS, 437, L21
Dotter, A., Sarajedini, A., Anderson, J., et al. 2010, ApJ, 708, 698
Ferraro, F. R., Lanzoni, B., Dalessandro, E., et al. 2012, Natur, 492, 393
Gaia Collaboration, Helmi, A., van Leeuwen, F., et al. 2018, A&A, 616, A12
Gieles, M., Charbonnel, C., Krause, M. G. H., et al. 2018, MNRAS, 478, 2461
Glatt, K., Grebel, E. K., Jordi, K., et al. 2011, AJ, 142, 36
Goldsbury, R., Richer, H. B., Anderson, J., et al. 2010, AJ, 140, 1830
Harris, W. E. 1996, AJ, 112, 1487
Hénault-Brunet, V., Gieles, M., Agertz, O., & Read, J. I. 2015, MNRAS, 450, 1164
King, I. R. 1966, AJ, 71, 64
Krause, M. G. H., Charbonnel, C., Bastian, N., et al. 2016, A&A, 587, A53
Lanzoni, B., Ferraro, F. R., Alessandrini, E., et al. 2016, ApJL, 833, L29
Lardo, C., Bellazzini, M., Pancino, E., et al. 2011, A&A, 525, A114
Larsen, S. S., Brodie, J. P., Grundahl, F., & Strader, J. 2014, ApJ, 797, 15
Lucatello, S., Sollima, A., Gratton, R., et al. 2015, A&A, 584, A52
Lupton, R. 1993, Statistics in Theory and Practice (Princeton, NJ: Princeton Univ. Press)
Martocchia, S., Cabrera-Ziri, I., Lardo, C., et al. 2018a, MNRAS, 473, 2688
Martocchia, S., Niederhofer, F., Dalessandro, E., et al. 2018b, MNRAS, 477, 4696
Massari, D., Lapenna, E., Bragaglia, A., et al. 2016, MNRAS, 458, 4162
Miholics, M., Webb, J. J., & Sills, A. 2015, MNRAS, 454, 2166
Milone, A. P., Marino, A. F., Renzini, A., et al. 2018, MNRAS, 481, 5098
Milone, A. P., Piotto, G., Renzini, A., et al. 2017, MNRAS, 464, 3636
Monelli, M., Milone, A. P., Stetson, P. B., et al. 2013, MNRAS, 431, 2126
Mucciarelli, A., Carretta, E., Origlia, L., & Ferraro, F. R. 2008, AJ, 136, 375
Nardiello, D., Libralato, M., Piotto, G., et al. 2018, MNRAS, 481, 3382
Piotto, G., Bedin, L. R., Anderson, J., et al. 2007, ApJL, 661, L53
Piotto, G., Milone, A. P., Bedin, L. R., et al. 2015, AJ, 149, 91
Richer, H. B., Heyl, J., Anderson, J., et al. 2013, ApJL, 771, L15
Sbordone, L., Salaris, M., Weiss, A., & Cassisi, S. 2011, A&A, 534, A9
Schiavon, R. P., Caldwell, N., Conroy, C., et al. 2013, ApJL, 776, L7
Simioni, M., Milone, A. P., Bedin, L. R., et al. 2016, MNRAS, 463, 449
Stetson, P. B., Pancino, E., Zocchi, A., Sanna, N., & Monelli, M. 2019, MNRAS, 485, 3042
Tiongco, M. A., Vesperini, E., & Varri, A. L. 2019, MNRAS, 487, 5535
Vesperini, E., Hong, J., Webb, J. J., et al. 2018, MNRAS, 476, 2731
Vesperini, E., McMillan, S. L. W., D'Antona, F., & D'Ercole, A. 2013, MNRAS, 429, 1913